Supplementary Information

Towards kinetic control of coordination self-assembly: A case study of a Pd_3L_6 double-walled triangle to predict the outcomes by a reaction network model

Satoshi Takahashi,*[1] Tomoki Tateishi,[1] Yuya Sasaki, [1] Hirofumi Sato[2,3,4] and Shuichi Hiraoka*[1]

[1]Department of Basic Science, Graduate School of Arts and Sciences
The University of Tokyo
3-8-1 Komaba, Meguro-ku, Tokyo 153-8902, Japan
[2]Department of Molecular Engineering, Kyoto University, Kyoto 615-8510, Japan.
[3]Elements Strategy Initiative for Catalysts and Batteries, Kyoto University, Kyoto 615-8510, Japan.
[4]Fukui Institute for Fundamental Chemistry, Kyoto University, Kyoto 606-8103, Japan

E-mail: takahasi@mns2.c.u-tokyo.c.jp, hiraoka-s@g.ecc.u-tokyo.ac.jp

Contents

General Information

^{1}H, ^{1}H DOSY and H-H COSY spectra were recorded using a Bruker AV-500 (500 MHz) spectrometer. All ^{1}H spectra were referenced using a residual solvent peak, CD_3NO_2 (δ 4.33). Electrospray ionization time-of-flight (ESI-TOF) mass spectra were obtained using a Waters Xevo G2-S Tof mass spectrometer. Geometry optimizations were performed by density functional theory (DFT) with *m*-GGA (M06-L) functional (BIOVIA Material Studio 2017 R2, Accelrys Software Inc.).

Materials

Unless otherwise noted, all solvents and reagents were obtained from commercial suppliers (TCI Co., Ltd., WAKO Pure Chemical Industries Ltd., KANTO Chemical Co., Inc. and Sigma-Aldrich Co.) and were used as received. CD_3NO_2 was purchased from Acros Organics and used after dehydration with Molecular Sieves 4Å. Ditopic ligand **1**[1] and $[PdPy^*_4](BF_4)_2$[2] were prepared according to the literature.

Numerical analysis of self-assembly process (NASAP)

The minimal reaction network

For our numerical analysis, a reaction network for the self-assembly of the M_3L_6 double-walled triangle (DWT, Figure 2a) is constructed as follows. Starting from the final product M_3L_6 (3,6,0) (a shorthand notation is used as in the main text, that is, (a,b,c) for $M_aL_bX_c$), the reaction path is traced back to the reactants, that is, MX_4 and L. In this back propagation process, all the directly available molecular species by a single ligand exchange are considered as the intermediates, so that the species consisting of more components than the (3,6,0) ($M_aL_bX_c$, $a\geq3$, $b\geq6$) are excluded from this network. With this procedure taken, it is found that the total of 161 molecular species (including both the reactants and the products themselves) construct a minimal reaction network composed of 896 reactions, each of which contains the forward and backward processes. We refrain showing the minimal reaction network with all the possible structures of intermediate species, because it is too complicated to facilitate our grabbing the picture of the self-assembly process. Instead, a simplified network is displayed in Figure 3 with the possible compositions alone. All the elementary reactions considered in this study are given in Table S1.

Division of chemical reactions

Although we call it minimal, this reaction network turns out to be still so large that it is impossible to assign individual rate constants to each reactions and to search for the parameter set in such a vast parameter space to fit the experimental results best. Therefore, we divide the whole network into nine classes possessing similar characteristics and define rate constants as follows (Figure 2d):

i. Growth of oligomers.
   1. The first reaction expected to occur between the substrates for allowing the entire self-assembly reactions, that is, (1,0,4) + **1** → (1,1,3) + Py*: k_1 [min^{-1} M^{-1}] and k_{-1} [min^{-1} M^{-1}] for forward and backward reactions, respectively.
   2. Reactions (1,1,3) + **1** → (1,2,2) + Py^*, having *cis*- and *trans*-isomers: k_2 [min^{-1} M^{-1}] and k_{-2} [min^{-1} M^{-1}].
   3. Reactions between (1,2,2) (both *cis*- and *trans*-) and **1**, and between (1,3,1) and **1**: k_3 [min^{-1} M^{-1}] and k_{-3} [min^{-1} M^{-1}].
   4. Reactions between those species with two or three Pd(II) centers and **1**, and among species with one Pd(II) center, leading to the ones with two Pd(II) centers: k_4 [min^{-1} M^{-1}] and k_{-4} [min^{-1} M^{-1}].
   5. Reactions between the species with two Pd(II) centers and those with one Pd(II) center, leading to the species with three Pd(II) centers: k_5 [min^{-1} M^{-1}] and k_{-5} [min^{-1} M^{-1}].
   6. The next-to-last is given a special treatment, that is, (3,5,2) + **1** → (3,6,1) + Py*: k_6 [min^{-1} M^{-1}] and k_{-6} [min^{-1} M^{-1}].

ii. Double-wall making.
    7. Double-wall making except the final step: k_7 [min^{-1}] and k_{-7} [min^{-1} M^{-1}].
    8. The very final step of the DWT formation, (3,6,1) → (3,6,0) + Py*: k_8 [min^{-1}] and k_{-8} [min^{-1} M^{-1}].
iii. Cyclization.
    9. Cyclization of acyclic oligomers with three Pd(II) centers: k_9 [min^{-1}] and k_{-9} [min^{-1} M^{-1}].

Note that reactions in class (i) are the intermolecular ligand exchange and those in classes (ii) and (iii) are intramolecular. We have defined each rate constant as being per reaction site, so that the actual reaction rate constant for each reaction is estimated as the above constant multiplied by the total number of available combinations. For example, for a ligand exchange reaction between MX_4 and a ditopic ligand L to produce MLX_3 and X, the rate constant is given as k_1 times 4 (the number of M-X bonds in MX_4) times 2 (the number of coordination sites in L), i.e.,

$$MX_4 + L \xrightarrow{8k_1} MLX_3 + X.$$

We adopted this setting to explicitly distinguish the structural difference among the species with the same composition.

In order to numerically track the time evolution of the existence ratios for both reactants and products and the ($\langle n \rangle$, $\langle k \rangle$) values, we have adopted a stochastic approach based on the chemical master equation, the so-called Gillespie algorithm. In this algorithm, for all the possible N chemical reactions including molecular species S_{ai}, S_{bi}, S_{ci}, ...,

$$S_{ai} + S_{bi} + \ldots \rightarrow S_{ci} + \ldots (i = 1, \ldots, N),$$

the total reaction rate R_{tot} is calculated as

$$R_{tot} = r_1 + r_2 + \cdots + r_N,$$

$$r_i = k_i[S_{ai}][S_{bi}] \ldots.$$

Starting from the initial time $t = 0$, at each instant t, which one of the reactions to occur is determined with the uniform random number $s_1 \in (0,1)$ as

if $s_1 \leq \frac{r_1}{R_{tot}}$, then reaction 1 occurs,

if $\frac{r_1}{R_{tot}} < s_1 \leq \frac{r_1 + r_2}{R_{tot}}$, then reaction 2 occurs,

if $\frac{r_1 + \cdots + r_{N-1}}{R_{tot}} < s_1 \leq 1$, then reaction N occurs.

Another uniform random number $s_2 \in (0,1)$ is independently given to fix the time incremental dt as

$$dt = \ln(1/s_2)/R_{tot}.$$

Time is updated as $t = t + dt$, together with the update of the numbers of corresponding molecular species, i.e., $\langle S_{ai} \rangle \rightarrow \langle S_{ai} \rangle - 1$, $\langle S_{bi} \rangle \rightarrow \langle S_{bi} \rangle - 1$, $\langle S_{ci} \rangle \rightarrow \langle S_{ci} \rangle + 1$, …. The reason why this approach traces the chemical reactions and actually works well is given in the literature in detail, along with the practical way to implement it.[3–6]

With initial conditions (numbers of species), $\langle [PdPy^*_4]^{2+} \rangle_0 = 1{,}200$, $\langle \mathbf{1} \rangle_0 = 2{,}400$ and $\langle \text{others} \rangle_0 = 0$, rate constant search was performed in an eighteen-dimensional parameter space (k_1, k_{-1}, k_2, k_{-2}, …, k_9, k_{-9}). The Avogadro number and the volume of the simulation box were set to be $N_A = 6.0 \times 10^{23}$ and $V = 2.5 \times 10^{-18}$ L, respectively, which give the same concentration as the experiments were carried out under ($[Pd]_0 = 0.80$ mM and $[\mathbf{1}]_0 = 1.6$ mM). After the rate constant search was finished, refined simulations were performed for some rate parameter sets that give existence ratios and ($\langle n \rangle$, $\langle k \rangle$) plot in good agreement with the experimental counterparts. Representative results were shown in figures of the main text, in which the initial particles and the volume of the simulation box were set to be a hundred times larger than the rough parameter search, i.e.,

$\langle[PdPy^*_4]^{2+}\rangle_0$ = 120,000, $\langle \mathbf{1} \rangle_0$ = 240,000, and V = 2.5 × 10^{-16} L. Although the numerical results of a single simulation are shown in the figures, convergence behavior was confirmed with several runs for the particle numbers given above.

Table S1. Chemical reactions considered in the minimal reaction network are classified into 83 groups due to their compositions.

Reaction label		Reaction label	
1	(3,6,1) ⇄ (3,6,0) + Py*	31	(2,5,1) + **1** ⇄ (2,6,0) + Py*
2	(3,5,2) + **1** ⇄ (3,6,1) + Py*	32	(2,6,1) ⇄ (2,6,0) + Py*
3	(3,6,2) ⇄ (3,6,1) + Py*	33	(2,4,2) + **1** ⇄ (2,5,1) + Py*
4	(3,5,3) ⇄ (3,5,2) + Py*	34	(2,5,2) ⇄ (2,5,1) + Py*
5	(3,5,3) + **1** ⇄ (3,6,2) + Py*	35	(2,3,3) + **1** ⇄ (2,4,2) + Py*
6	(3,6,3) ⇄ (3,6,2) + Py*	36	(2,4,3) ⇄ (2,4,2) + Py*
7	(3,4,4) + **1** ⇄ (3,5,3) + Py*	37	(2,2,4) + **1** ⇄ (2,3,3) + Py*
8	(3,5,4) ⇄ (3,5,3) + Py*	38	(2,3,4) ⇄ (2,3,3) + Py*
9	(3,4,5) ⇄ (3,4,4) + Py*	39	(2,2,5) ⇄ (2,2,4) + Py*
10	(3,5,4) + **1** ⇄ (3,6,3) + Py*	40	(3,5,5) + **1** ⇄ (3,6,4) + Py*
11	(2,4,2) + (1,2,2) ⇄ (3,6,3) + Py*	41	(2,5,2) + (1,1,3) ⇄ (3,6,4) + Py*
12	(2,3,3) + (1,3,1) ⇄ (3,6,3) + Py*	42	(2,4,3) + (1,2,2) ⇄ (3,6,4) + Py*
13	(3,6,4) ⇄ (3,6,3) + Py*	43	(2,3,4) + (1,3,1) ⇄ (3,6,4) + Py*
14	(2,5,1) + (1,1,3) ⇄ (3,6,3) + Py*	44	(3,4,6) + **1** ⇄ (3,5,5) + Py*
15	(3,4,5) + **1** ⇄ (3,5,4) + Py*	45	(2,4,3) + (1,1,3) ⇄ (3,5,5) + Py*
16	(2,4,2) + (1,1,3) ⇄ (3,5,4) + Py*	46	(2,3,4) + (1,2,2) ⇄ (3,5,5) + Py*
17	(2,3,3) + (1,2,2) ⇄ (3,5,4) + Py*	47	(2,6,1) + (1,0,4) ⇄ (3,6,4) + Py*
18	(3,5,5) ⇄ (3,5,4) + Py*	48	(2,2,5) + (1,4,0) ⇄ (3,6,4) + Py*
19	(2,6,0) + (1,0,4) ⇄ (3,6,3) + Py*	49	(2,5,2) + (1,0,4) ⇄ (3,5,5) + Py*
20	(2,5,1) + (1,0,4) ⇄ (3,5,4) + Py*	50	(2,2,5) + (1,3,1) ⇄ (3,5,5) + Py*
21	(3,3,6) + **1** ⇄ (3,4,5) + Py*	51	(3,3,7) + **1** ⇄ (3,4,6) + Py*
22	(2,4,2) + (1,0,4) ⇄ (3,4,5) + Py*	52	(2,4,3) + (1,0,4) ⇄ (3,4,6) + Py*
23	(2,3,3) + (1,1,3) ⇄ (3,4,5) + Py*	53	(2,3,4) + (1,1,3) ⇄ (3,4,6) + Py*
24	(3,4,6) ⇄ (3,4,5) + Py*	54	(2,2,5) + (1,2,2) ⇄ (3,4,6) + Py*
25	(2,2,4) + (1,4,0) ⇄ (3,6,3) + Py*	55	(2,1,6) + (1,4,0) ⇄ (3,5,5) + Py*
26	(2,2,4) + (1,3,1) ⇄ (3,5,4) + Py*	56	(2,1,6) + (1,3,1) ⇄ (3,4,6) + Py*
27	(2,2,4) + (1,2,2) ⇄ (3,4,5) + Py*	57	(2,3,4) + (1,0,4) ⇄ (3,3,7) + Py*
28	(2,3,3) + (1,0,4) ⇄ (3,3,6) + Py*	58	(2,2,5) + (1,1,3) ⇄ (3,3,7) + Py*
29	(2,2,4) + (1,1,3) ⇄ (3,3,6) + Py*	59	(3,2,8) + **1** ⇄ (3,3,7) + Py*
30	(3,3,7) ⇄ (3,3,6) + Py*	60	(2,1,6) + (1,2,2) ⇄ (3,3,7) + Py*

Table S1. Continued.

Reaction label		Reaction label	
61	(2,5,2) + **1** ⇄ (2,6,1) + Py*	73	(1,3,1) + (1,0,4) ⇄ (2,3,4) + Py*
62	(1,4,0) + (1,2,2) ⇄ (2,6,1) + Py*	74	(2,1,6) + **1** ⇄ (2,2,5) + Py*
63	(1,3,1) + (1,3,1) ⇄ (2,6,1) + Py*	75	(1,2,2) + (1,0,4) ⇄ (2,2,5) + Py*
64	(2,4,3) + **1** ⇄ (2,5,2) + Py*	76	(1,1,3) + (1,1,3) ⇄ (2,2,5) + Py*
65	(1,3,1) + (1,2,2) ⇄ (2,5,2) + Py*	77	(2,2,5) + (1,0,4) ⇄ (3,2,8) + Py*
66	(2,3,4) + **1** ⇄ (2,4,3) + Py*	78	(2,1,6) + (1,1,3) ⇄ (3,2,8) + Py*
67	(1,3,1) + (1,1,3) ⇄ (2,4,3) + Py*	79	(1,1,3) + (1,0,4) ⇄ (2,1,6) + Py*
68	(1,2,2) + (1,2,2) ⇄ (2,4,3) + Py*	80	(1,3,1) + **1** ⇄ (1,4,0) + Py*
69	(1,4,0) + (1,1,3) ⇄ (2,5,2) + Py*	81	(1,2,2) + **1** ⇄ (1,3,1) + Py*
70	(2,2,5) + **1** ⇄ (2,3,4) + Py*	82	(1,1,3) + **1** ⇄ (1,2,2) + Py*
71	(1,2,2) + (1,1,3) ⇄ (2,3,4) + Py*	83	(1,0,4) + **1** ⇄ (1,1,3) + Py*
72	(1,4,0) + (1,0,4) ⇄ (2,4,3) + Py*		

Reaction flow rate and its accumulation

Due to the approximate unidirectionality of the middle stage of the self-assembly (see Figure 4d), we can simply count the number of reactions for each listed in Table 1 to (approximately) obtain how many molecules were produced in the course of the global reaction. Comparing the ratio of the total number of each actually produced intermediate to $\langle \mathbf{1} \rangle_0$ divided by that contained in a single molecule of that species (maximum possible number) (see the caption of Figure 5a), it is revealed what kind of reactions dominate the self-assembly process. The result is shown in Figure S1, which indicates that all the reactions do not equally contribute to the formation of the $[Pd_3\mathbf{1}_6]^{6+}$ DWT. The height of each bar in this figure is reflected in the thickness of arrows in Figure 6.

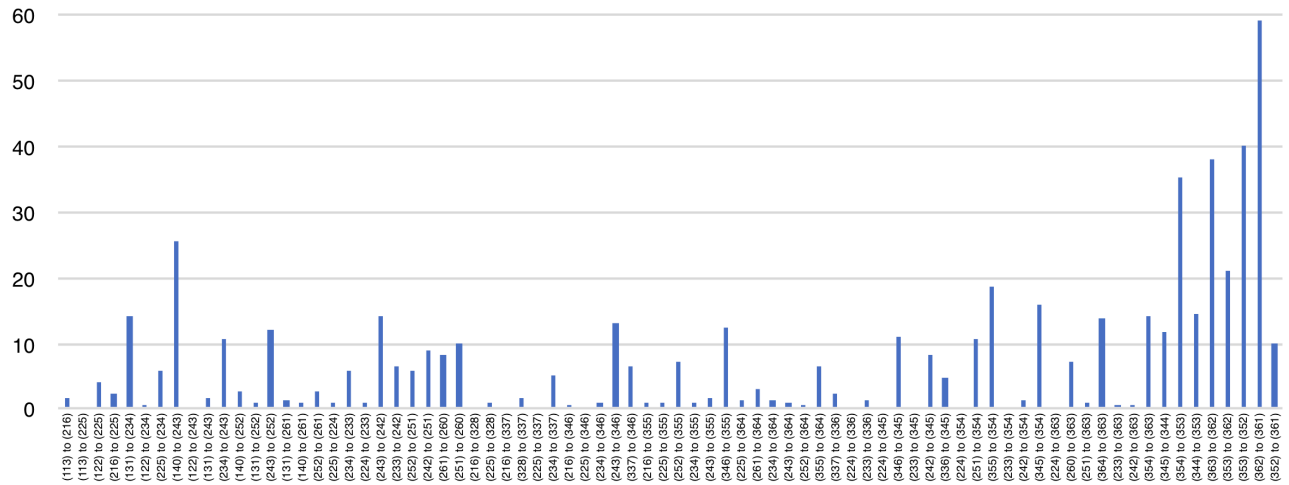

Figure S1. Accumulation of reaction flow rate for each reaction (unit in %), with the denominator being the maximum possible number of the product composition.

Di- and Trinuclear intermediates convertible to double-walled structure

Figure S2 indicates the schematic representation of dinuclear intermediates that can produce a double-walled structure via intramolecular ligand exchange. Although not all the species are dominant, these allow the double-wall making (***d*1**) to precede the cyclization (***c***). Schematic representation is given in Figure S3 for trinuclear species without double-walled structure. It should be noted that those species with only the possibility of either double-wall making or cyclization are excluded here. The similar representation for trinuclear species with a singly double-walled structure is given in Figure S4, in which those with only the possibility of either double-wall making or cyclization are excluded.

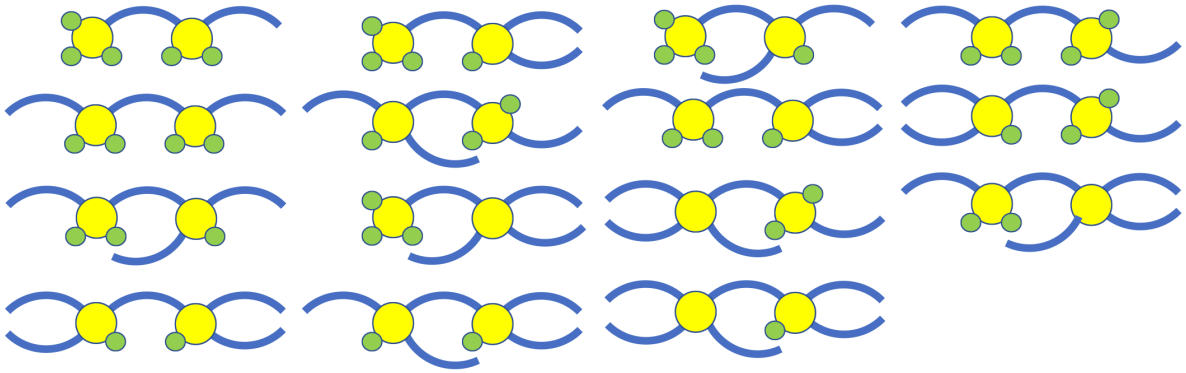

Figure S2. Schematic representation of dinuclear species convertible to double-walled ones. Cyclization cannot occur for these intermediates. What each pictorial figure indicates is the same as in Figure 2b.

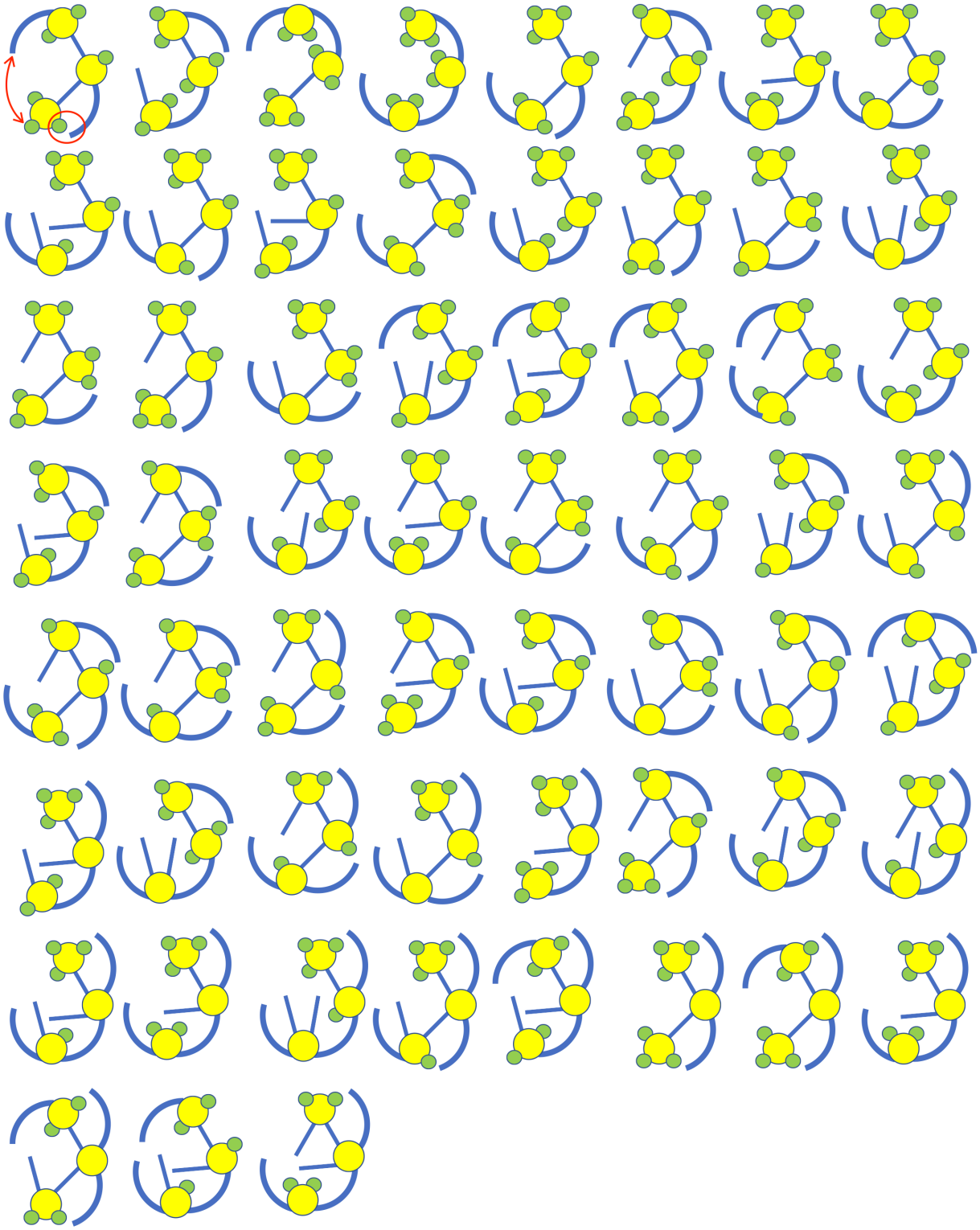

Figure S3. Schematic representation of trinuclear species without double-wall. Examples for the reaction point are shown at the upper-left corner with an ellipse and a double-headed arrow for double-wall making and cyclization, respectively. Considering that we assume the free rotation around the Pd(II)-**1** bond, the ratio of reaction points for the double-wall making to those for the cyclization can be obtained as 188:148 by a simple counting. What each pictorial figure indicates is the same as in Figure 2b.

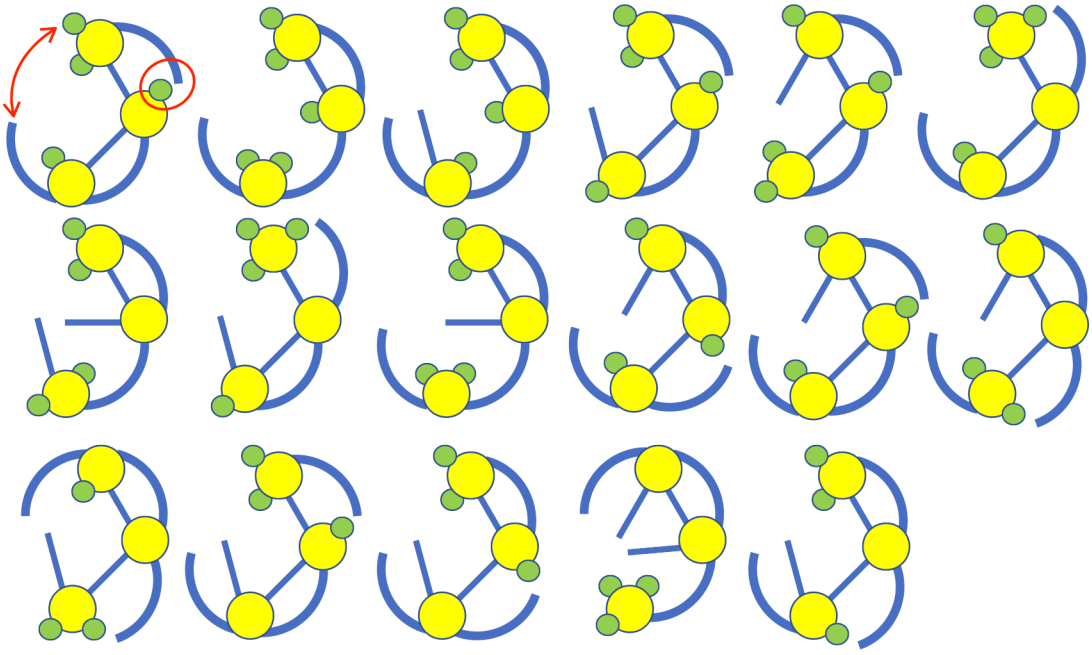

Figure S4. Schematic representation of trinuclear species with a singly double-walled structure. Examples for the reaction point are shown at the upper-left corner with an ellipse and a double-headed arrow for double-wall making and cyclization, respectively. Considering that we assume the free rotation around the Pd(II)-**1** bond, the ratio of reaction points for the double-wall making to those for the cyclization can be obtained as 25:32 by a simple counting. What each pictorial figure indicates is the same as in Figure 2b.

Monitoring of the self-assembly of DWT by ^{1}H NMR

Procedure for monitoring the self-assembly process of the $[Pd_3\mathbf{1}_6]^{6+}$ double-walled triangle (DWT)

A 2.4 mM solution of [2.2]paracyclophane in $CHCl_3$ (125 μL), which was used as an internal standard, was added to two NMR tubes (tubes **I** and **II**) and the solvent was removed in vacuo. A solution of $[PdPy^*_4](BF_4)_2$ (12 mM) in CD_3NO_2 was prepared (solution **A**). Solution **A** (50 μL) and CD_3NO_2 (450 μL) were added to tube **I**. The exact concentration of $[PdPy^*_4](BF_4)_2$ in solution **A** was determined through the comparison of the signal intensity with [2.2]paracyclophane by ^{1}H NMR. A solution of ditopic ligand **1** (24 mM (for $[\mathbf{1}]_0/[Pd]_0$ = 4.0), 15 mM (for $[\mathbf{1}]_0/[Pd]_0$ = 2.5), 6.0 mM (for $[\mathbf{1}]_0/[Pd]_0$ = 1.0) and 3.0 mM (for $[\mathbf{1}]_0/[Pd]_0$ = 0.5)) in $CHCl_3$ (100 μL) was added to tube **II** and the solvent was removed in vacuo. Then CD_3NO_2 (500 μL) was added to tube **II** and the exact amount of **1** in tube **II** was determined through the comparison of the signal intensity with [2.2]paracyclophane by ^{1}H NMR. 0.25 eq. (for $[\mathbf{1}]_0/[Pd]_0$ = 4.0), 0.4 eq. (for $[\mathbf{1}]_0/[Pd]_0$ = 2.5), 1.0 eq. (for $[\mathbf{1}]_0/[Pd]_0$ = 1.0) and 2.0 eq. (for $[\mathbf{1}]_0/[Pd]_0$ = 0.5) (against the amount of ligand **1** in tube **II**) of solution **A** (*ca.* 50 μL; the exact amount was determined based on the exact concentrations of solution **A** and of **1** in tube **II**) was added to tube **II** at 263 K. The self-assembly of the $[Pd_3\mathbf{1}_6]^{6+}$ DWT in each stoichiometric ratio ($[\mathbf{1}]_0/[Pd]_0$ = 0.5, 1.0, 2.5, and 4.0) was monitored at 298 K by ^{1}H NMR spectroscopy. The ^{1}H NMR spectra for these experiments are shown in Figures 12 and S8. After the convergence of the self-assembly at 298 K, the reaction mixtures were heated at 343 K and monitored by ^{1}H NMR spectroscopy, the ^{1}H NMR spectra of which are shown in Figure S11. The exact ratio of **1** and $[PdPy^*_4](BF_4)_2$ was unambiguously determined by the comparison of the integral value of each ^{1}H signal of [2.2]paracyclophane. The amounts of **1**, $[PdPy^*_4](BF_4)_2$, the $[Pd_3\mathbf{1}_6]^{6+}$ DWT and Py* (and the long-lived intermediates (2,2,4) (for $[\mathbf{1}]_0/[Pd]_0$ = 0.5)) were quantified by the integral value of each ^{1}H signal against the signal of the internal standard ([2.2]paracyclophane). The data, the average values of the existence ratios and the ($\langle n \rangle$, $\langle k \rangle$) values are listed in Tables S3–S6.

Determination of the existence ratios of each species

The relative integral value of each ^{1}H NMR signal against the internal standard [2.2]paracyclophane is used as the integral value in this description. We define the integral values of the signal for the substrates and the products at each time *t* as follows:

$I_L(t)$: 1/4 of the integral value of the *a* proton in free ligand **1**
$I_M(t)$: the integral value of the *h* proton of Py* in $[PdPy*_4]^{2+}$
$I_{\mathbf{DWT}}(t)$: 1/4 of the integral value of the *a* proton in the $[Pd_3\mathbf{1}_6]^{6+}$ DWT
$I_{224}(t)$: 1/2 of the integral value of the *h* proton in the long-lived intermediates (2,2,4) (for $[\mathbf{1}]_0/[Pd]_0 = 0.5$)
$I_{Py*}(t)$: the integral value of the *g* proton of free Py*

$I_M(0)$ was determined based on the exact concentration of solution **A** determined by ^{1}H NMR and the exact volume of solution **A** added into tube **II**.
$I_L(0)$ was determined by ^{1}H NMR measurement before the addition of solution **A** into tube **II**.

Existence ratio of $[PdPy*_4]^{2+}$

As the total amount of $[PdPy*_4]^{2+}$ corresponds to $I_M(0)$, the existence ratio of $[PdPy*_4]^{2+}$ at *t* is expressed by $I_M(t)/I_M(0)$.

Existence ratio of **1**

As the total amount of free ligand **1** corresponds to $I_L(0)$, the existence ratio of **1** at *t* is expressed by $I_L(t)/I_L(0)$.

Existence ratio of the $[Pd_3\mathbf{1}_6]^{6+}$ DWT

($[\mathbf{1}]_0/[Pd]_0 \leq 2.0$) As the total amount of the $[Pd_3\mathbf{1}_6]^{6+}$ DWT is quantified based on **1**, the existence ratio of the $[Pd_3\mathbf{1}_6]^{6+}$ DWT at *t* is expressed by $I_{\mathbf{DWT}}(t)/I_L(0)$.
($[\mathbf{1}]_0/[Pd]_0 = 2.5$) As the total amount of the $[Pd_3\mathbf{1}_6]^{6+}$ DWT is quantified based on Pd^{2+} ions, the existence ratio of the $[Pd_3\mathbf{1}_6]^{6+}$ DWT at *t* is expressed by $I_{\mathbf{DWT}}(t)/(I_L(0)\times 2/2.5)$.
($[\mathbf{1}]_0/[Pd]_0 = 4.0$) As well as $[\mathbf{1}]_0/[Pd]_0 = 2.5$, the existence ratio of the $[Pd_3\mathbf{1}_6]^{6+}$ DWT at *t* is expressed by $I_{\mathbf{DWT}}(t)/(I_L(0)\times 2/4)$.

Existence ratio of Py*

As the total amount of Py* corresponds to $I_M(0)$, the existence ratio of Py* at *t* is expressed by $I_{Py*}(t)/I_M(0)$.

Existence ratio of the species (2,2,4) (for $[\mathbf{1}]_0/[Pd]_0 = 0.5$)

As the total amount of the species (2,2,4) is quantified based on **1**, the existence ratio of the species (2,2,4) at *t* is expressed by $I_{224}(t)/I_L(0)$.

Existence ratio of the total intermediates not observed by ^{1}H NMR (**Int**)

The existence ratio of the total intermediates not observed by ^{1}H NMR (**Int**) is determined based on the amount of ligand **1** in **Int**. Thus the existence ratio of **Int** is calculated by subtracting the other species containing **1** (free **1** and the $[Pd_3\mathbf{1}_6]^{6+}$ DWT) from the total amount of **1** ($I_L(0)$). The existence ratio of **Int** at *t* is expressed by $(I_L(0) - I_L(t) - I_{\mathbf{DWT}}(t))/I_L(0)$.
Note that the definition of the existence ratio of **Int** is the same despite different initial stoichiometries; for $[\mathbf{1}]_0/[Pd]_0 = 0.5$, the existence ratio of **Int** does not include the species (2,2,4); for $[\mathbf{1}]_0/[Pd]_0 = 2.5$ and $[\mathbf{1}]_0/[Pd]_0 = 4.0$, the sum of the existence ratios of free **1**, DWT and **Int** is not equal to 100% because the existence ratio

of the $[Pd_3\mathbf{1}_6]^{6+}$ DWT was quantified based on Pd^{2+} ions under the conditions.

⟨*a*⟩
The total amount of Pd^{2+} ions corresponds to $I_M(0)/4$. The amount of Pd^{2+} ions in $[PdPy^*_4]^{2+}$ at t corresponds to $I_M(t)/4$. The amount of Pd^{2+} ions in the $[Pd_3\mathbf{1}_6]^{6+}$ DWT at t corresponds to $I_{\mathbf{DWT}}(t)/2$. The amount of Pd^{2+} ions in **Int** at t is thus expressed by $I_M(0)/4 - I_M(t)/4 - I_{\mathbf{DWT}}(t)/2$.

⟨*b*⟩
The total amount of ligand **1** corresponds to $I_L(0)$. The amount of free ligand **1** at t corresponds to $I_L(t)$. The amounts of ligand **1** in the $[Pd_3\mathbf{1}_6]^{6+}$ DWT at t corresponds to $I_{\mathbf{DWT}}(t)$. The amount of ligand **1** in **Int** at t is thus expressed by $I_L(0) - I_L(t) - I_{\mathbf{DWT}}(t)$.

⟨*c*⟩
The total amount of Py* corresponds to $I_M(0)$. The amount of free Py* at t corresponds to $I_{Py^*}(t)$. The amount of Py* in $[PdPy^*_4]^{2+}$ at t corresponds to $I_M(t)$. The amount of Py* in **Int** at t is thus expressed by $I_M(0) - I_{Py^*}(t) - I_M(t)$.

The ⟨*n*⟩ and ⟨*k*⟩ values are determined with these ⟨*a*⟩, ⟨*b*⟩ and ⟨*c*⟩ values by eqs. (1) and (2).

$$\langle n \rangle = \frac{4\langle a \rangle - \langle c \rangle}{\langle b \rangle} \quad (1)$$

$$\langle k \rangle = \frac{\langle a \rangle}{\langle b \rangle} \quad (2)$$

The existence ratios of **1**, $[PdPy^*_4](BF_4)_2$, the $[Pd_3\mathbf{1}_6]^{6+}$ DWT, the species (2,2,4), Py* and **Int**, and the ⟨*a*⟩–⟨*c*⟩ and the (⟨*n*⟩, ⟨*k*⟩) values in each stoichiometric ratio ($[\mathbf{1}]_0/[Pd]_0$ = 0.5, 1.0, 2.5, and 4.0) are listed in Tables S3–S6.

Characterization of the long-lived intermediate (2,2,4)

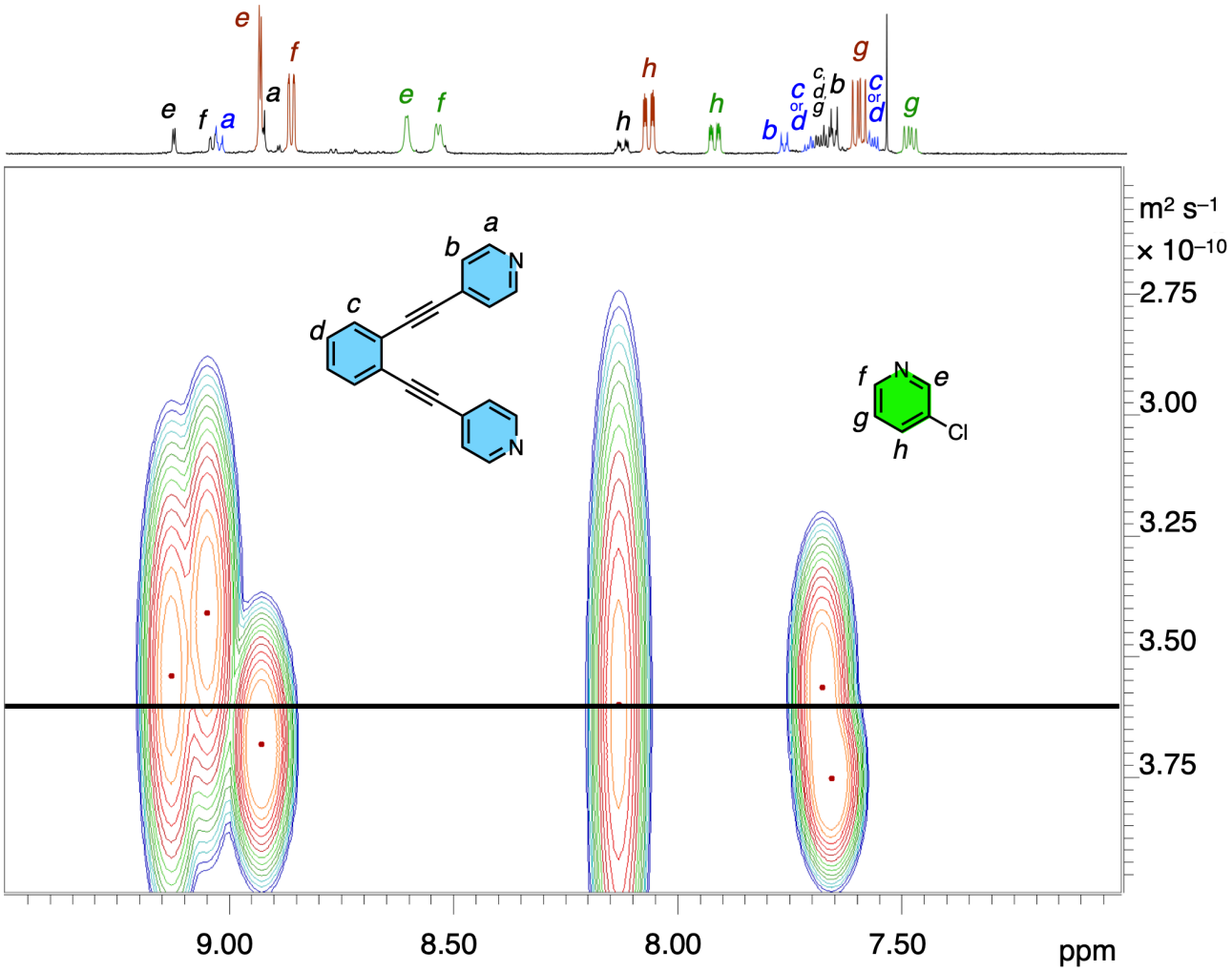

Figure S5. ^{1}H DOSY NMR spectrum (500 MHz, aromatic region, CD_3NO_2, 298 K) of the reaction mixture for the self-assembly of the $[Pd_3\mathbf{1}_6]^{6+}$ DWT from **1** and $[PdPy^*_4](BF_4)_2$ ($[Pd]_0$ = 1.0 mM, $[\mathbf{1}]_0/[Pd]_0$ = 0.5) at 298 K measured at 12 h. Signals colored in blue, brown and green indicate the $[Pd_3\mathbf{1}_6]^{6+}$ DWT, $[PdPy^*_4]$ $(BF_4)_2$ and Py*, respectively.

Table S2. A list of diffusion coefficients (D), errors, log$D$ and errors for log$D$ of the species (2,2,4).

Peak	F2 / ppm	D / m^2 s^{-1}	Error	log$D$	error for log$D$
e	9.128	3.54×10^{-10}	2.37×10^{-11}	–9.451	0.029
f	9.043	3.41×10^{-10}	2.21×10^{-11}	–9.467	0.028
a	8.923	3.69×10^{-10}	1.24×10^{-11}	–9.433	0.015
h	8.133	3.59×10^{-10}	3.76×10^{-11}	–9.445	0.046
c, *d*, *g*	7.675	3.56×10^{-10}	1.48×10^{-11}	–9.449	0.018
b	7.658	3.75×10^{-10}	9.34×10^{-12}	–9.426	0.011
Avg.		3.59×10^{-10}	2.00×10^{-11}	–9.445	0.024

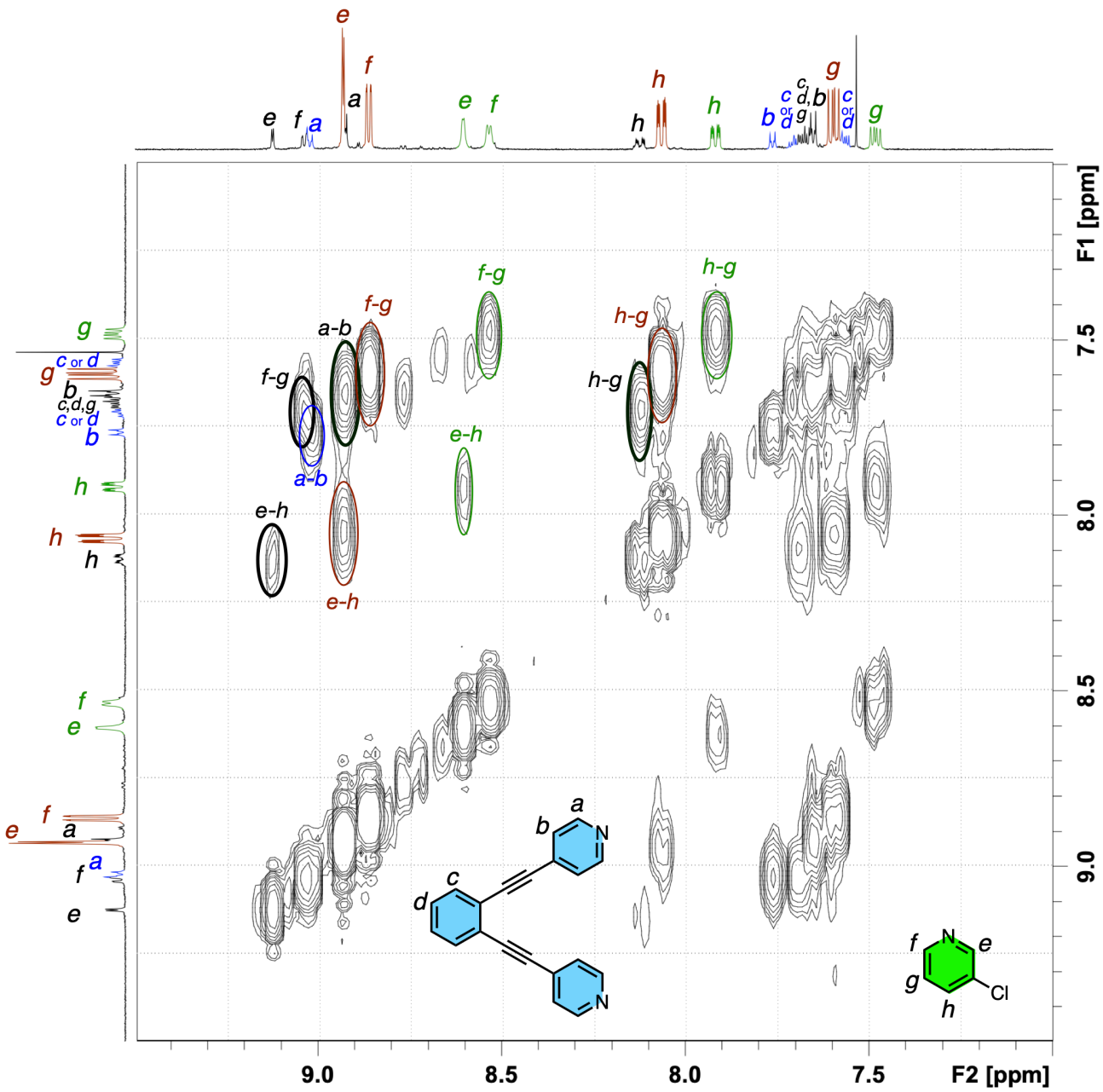

Figure S6. H-H COSY NMR spectrum (500 MHz, aromatic region, CD_3NO_2, 298 K) of the reaction mixture for the self-assembly of the $[Pd_3\mathbf{1}_6]^{6+}$ DWT from **1** and $[PdPy^*_4](BF_4)_2$ ($[Pd]_0$ = 1.0 mM, $[\mathbf{1}]_0/[Pd]_0$ = 0.5) at 298 K measured at 12 h. Signals colored in blue, brown and green indicate the $[Pd_3\mathbf{1}_6]^{6+}$ DWT, $[PdPy^*_4](BF_4)_2$ and Py*, respectively.

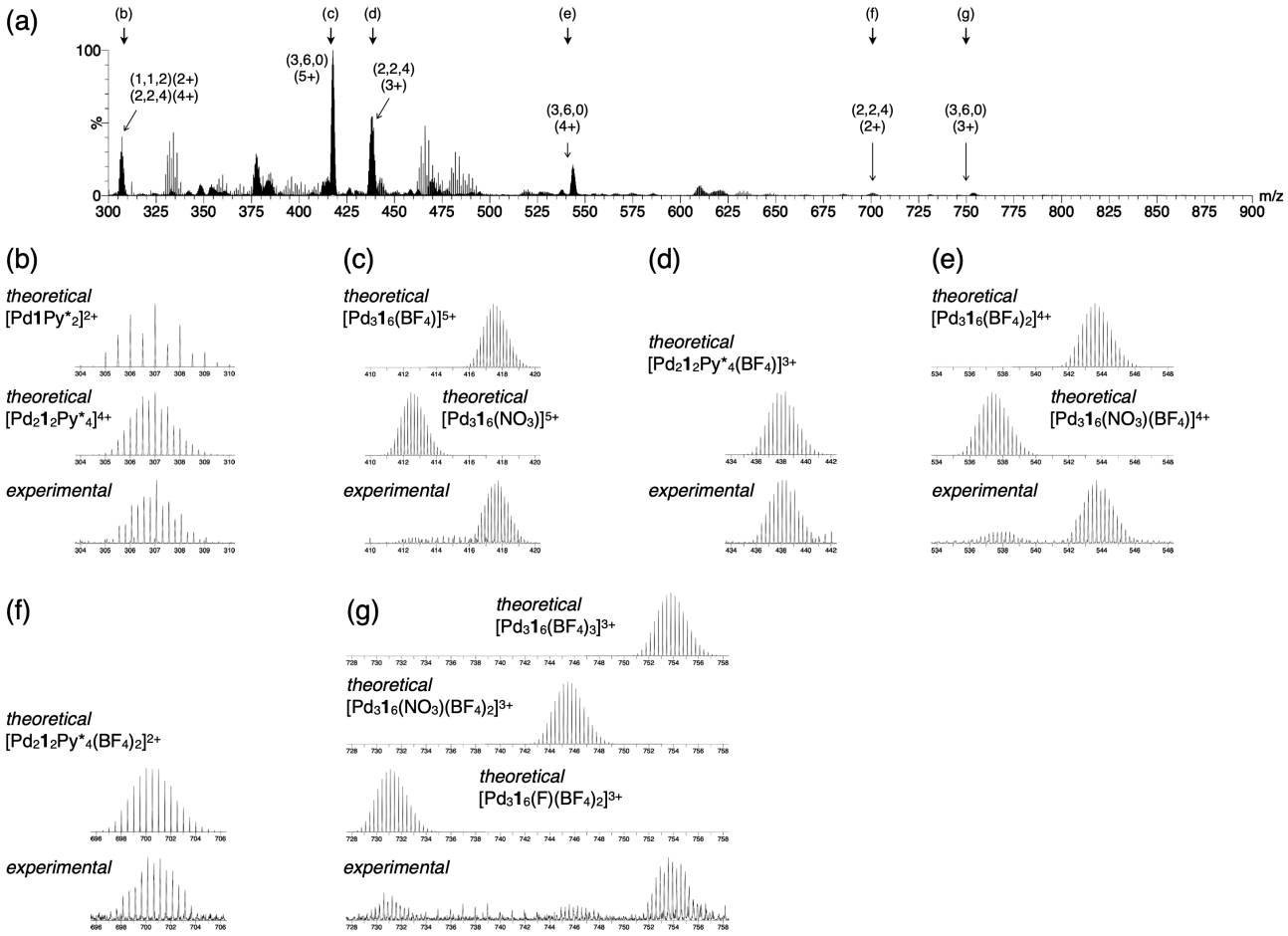

Figure S7. ESI-TOF mass spectra of the reaction mixture for the self-assembly of the $[Pd_3\mathbf{1}_6]^{6+}$ DWT from **1** and $[PdPy^*_4](BF_4)_2$ ($[Pd]_0$ = 1.0 mM, $[\mathbf{1}]_0/[Pd]_0$ = 0.5) at 298 K measured at 12 h. Measurement condition: Capillary / 1.5 kV; Sampling Cone / 30 V; Source Offset / 80 V; Source / 40 °C; Desolvation / 40 °C; Cone Gas / 50 L h^{-1}; Desolvation Gas / 800 L h^{-1}; Flow rate / 5.0 μL min^{-1}. (a) *m/z*: 300–900 ((*a*,*b*,*c*) indicates species $[Pd_a\mathbf{1}_bPy^*_c]^{2a+}$), (b) $[Pd\mathbf{1}Py^*_2]^{2+}$ and $[Pd_2\mathbf{1}_2Py^*_4]^{4+}$, (c) $[Pd_3\mathbf{1}_6(NO_3)]^{5+}$ and $[Pd_3\mathbf{1}_6(BF_4)]^{5+}$, (d) $[Pd_2\mathbf{1}_2Py^*_4(BF_4)]^{3+}$, (e) $[Pd_3\mathbf{1}_6(NO_3)(BF_4)]^{4+}$ and $[Pd_3\mathbf{1}_6(BF_4)_2]^{4+}$, (f) $[Pd_2\mathbf{1}_2Py^*_4(BF_4)_2]^{2+}$ and (g) $[Pd_3\mathbf{1}_6(F)(BF_4)_2]^{3+}$, $[Pd_3\mathbf{1}_6(NO_3)(BF_4)_2]^{3+}$ and $[Pd_3\mathbf{1}_6(BF_4)_3]^{3+}$.

Self-assembly of the DWT with different initial stoichiometries

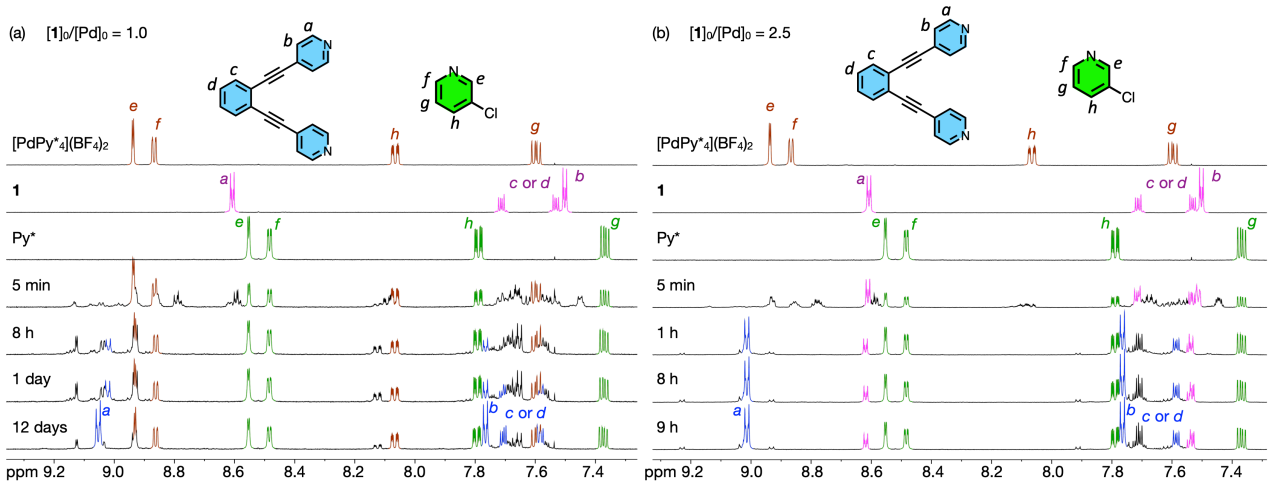

Figure S8. ^{1}H NMR spectra (500 MHz, aromatic region, CD_3NO_2, 298 K) of $[PdPy^*_4](BF_4)_2$, the ligand **1**, Py* and the reaction mixture for the self-assembly of the $[Pd_3\mathbf{1}_6]^{6+}$ DWT from $[PdPy^*_4](BF_4)_2$ ($[Pd]_0$ = 1.0 mM) and **1** in CD_3NO_2 at 298 K with different initial stoichiometries. (a) $[\mathbf{1}]_0/[Pd]_0$ = 1.0. (b) $[\mathbf{1}]_0/[Pd]_0$ = 2.5. The signals colored in blue, green, magenta and brown indicate the $[Pd_3\mathbf{1}_6]^{6+}$ DWT, Py*, **1** and $[PdPy^*_4](BF_4)_2$, respectively. The signal at 7.71 ppm was not colored because the either H^c or H^d signal of **1** and the either H^c or H^d signal of the $[Pd_3\mathbf{1}_6]^{6+}$ DWT are overlapped.

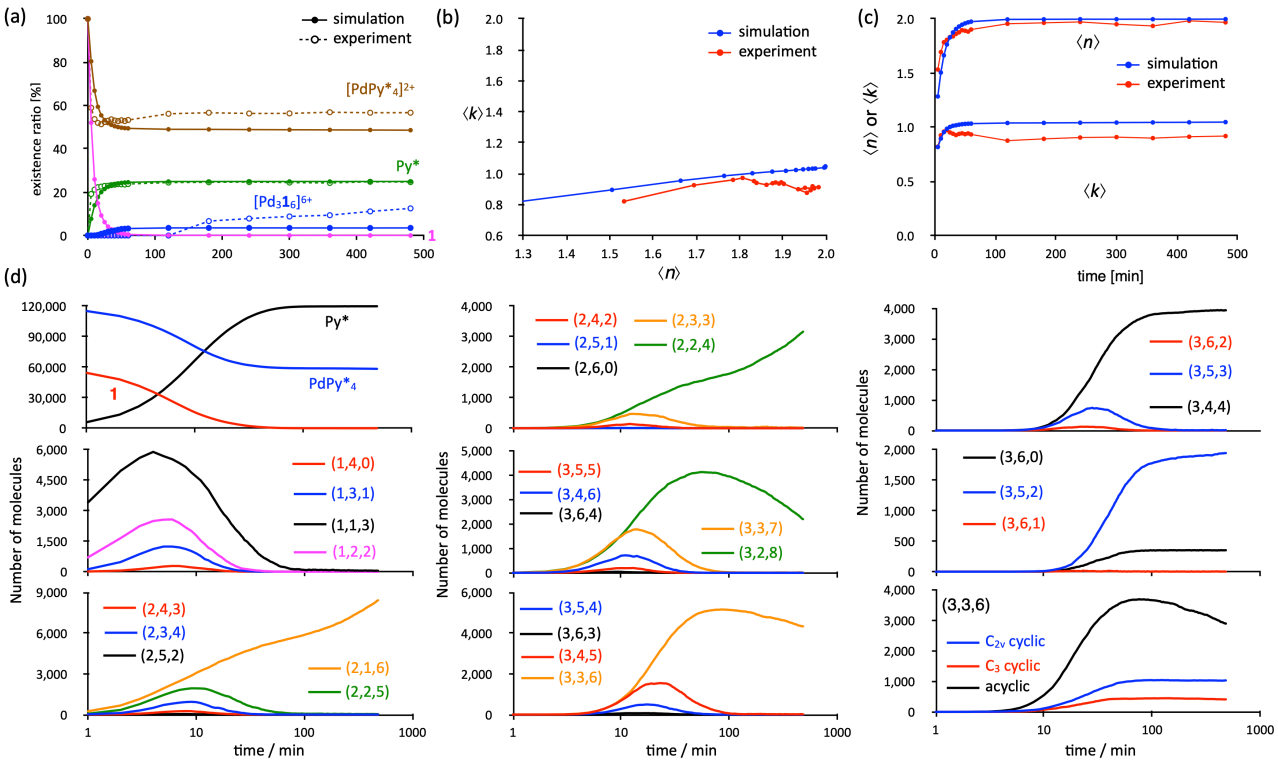

Figure S9. Numerical simulation of the self-assembly from **1** and $[PdPy^*_4]^{2+}$ in a 1:2 ratio ($[\mathbf{1}]_0/[Pd]_0$ = 0.5). (a) The existence ratios of the substrates and the products. (b) An *n*-*k* plot. (c) The $\langle n \rangle$ and $\langle k \rangle$ values with time. The experimental results are shown for comparison. (d) The number of species with time. The initial numbers of substrates are $\langle [PdPy^*_4]^{2+} \rangle_0$ = 120,000 and $\langle \mathbf{1} \rangle_0$ = 240,000.

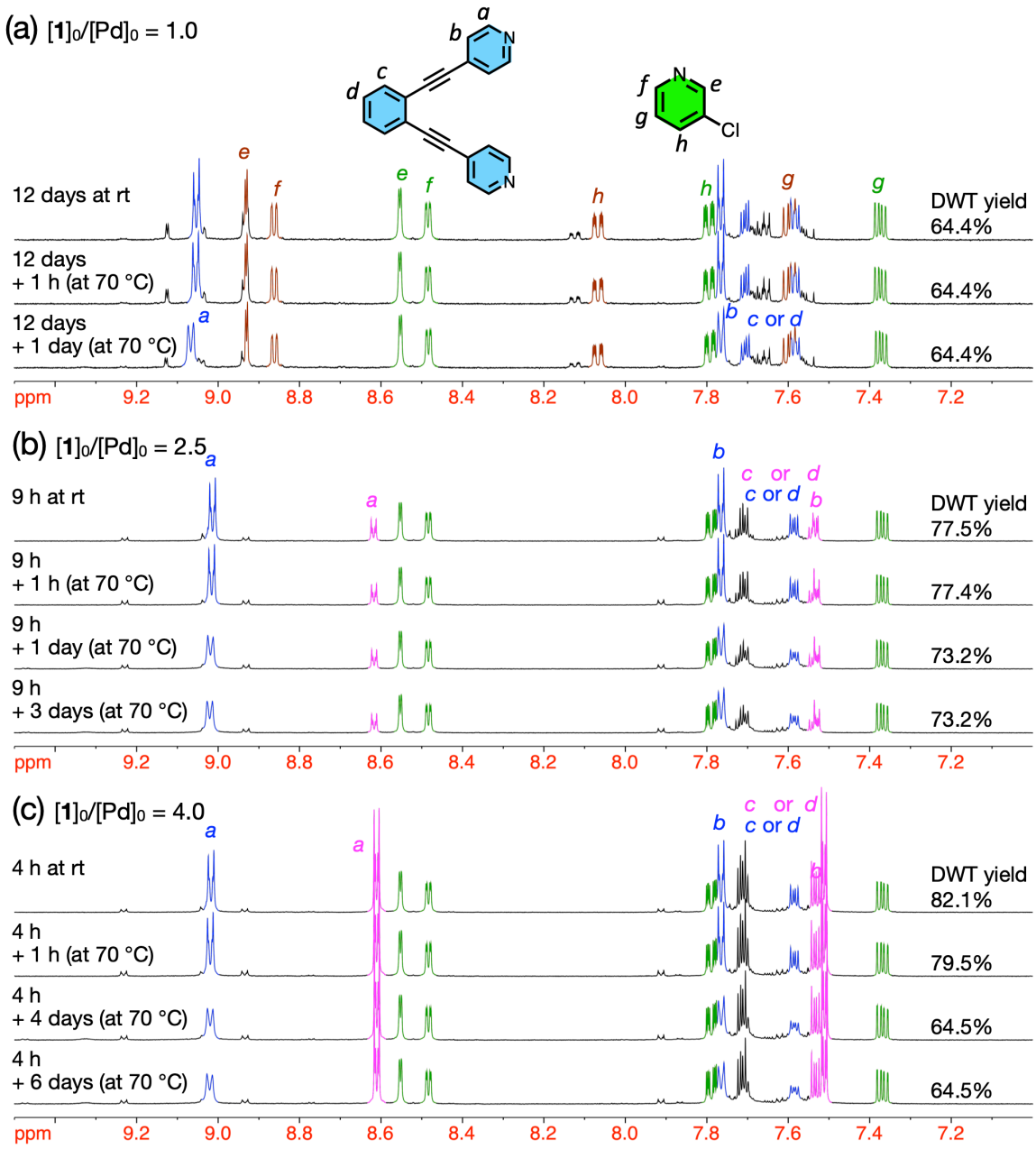

Figure S10. The change in the ^{1}H NMR spectrum of the reaction mixture of the self-assembly of the $[Pd_3\mathbf{1}_6]^{6+}$ DWT from **1** and $[PdPy^*_4](BF_4)_2$ ($[Pd]_0$ = 1.0 mM) in CD_3NO_2 by heating at 343 K after the convergence at 298 K. The initial stoichiometry is (a) $[\mathbf{1}]_0/[Pd]_0$ = 1.0, (b) $[\mathbf{1}]_0/[Pd]_0$ = 2.5 and (c) $[\mathbf{1}]_0/[Pd]_0$ = 4.0.

Time variation of **1**, $[PdPy^*_4](BF_4)_2$, the $[Pd_3\mathbf{1}_6]^{6+}$ DWT, Py*, **Int** and the ($\langle n\rangle$, $\langle k\rangle$) values for the self-assembly of the $[Pd_3\mathbf{1}_6]^{6+}$ DWT

Table S3. Time variation of **1**, $[PdPy^*_4](BF_4)_2$, the $[Pd_3\mathbf{1}_6]^{6+}$ DWT, the species (2,2,4), Py* and **Int**; $\langle a\rangle$–$\langle c\rangle$ values of the average composition of the intermediates ($[Pd_{\langle a\rangle}\mathbf{1}_{\langle b\rangle}Py^*_{\langle c\rangle}]^{2\langle a\rangle+}$); the ($\langle n\rangle$, $\langle k\rangle$) values for the self-assembly of the $[Pd_3\mathbf{1}_6]^{6+}$ DWT from $[PdPy^*_4](BF_4)_2$ ($[Pd]_0$ = 1.0 mM) and **1** ($[\mathbf{1}]_0$ = 0.5 mM) in CD_3NO_2 at 298 K with the initial stoichiometry of $[\mathbf{1}]_0/[Pd]_0$ = 0.5.

Time / min	**1** / %	$PdPy^*_4$ / %	DWT / %	(2,2,4) / %	Py* / %	**Int** / %	$\langle a\rangle$	$\langle b\rangle$	$\langle c\rangle$	$\langle n\rangle$	$\langle k\rangle$
0	100	100	0	0	0	0	—	—	—	—	—
5	0	59.0	0	26.0	19.2	100	0.091	0.111	0.195	1.533	0.821
10	0	53.7	0	31.8	21.2	100	0.103	0.111	0.224	1.694	0.925
15	0	52.0	0	32.9	22.3	100	0.107	0.111	0.229	1.784	0.960
20	0	51.4	0	34.9	22.6	100	0.108	0.111	0.232	1.807	0.972
25	0	52.4	0	36.8	22.9	100	0.106	0.111	0.220	1.833	0.952
30	0	53.0	0	39.3	23.0	100	0.105	0.111	0.214	1.839	0.940
35	0	53.6	0	40.1	23.3	100	0.103	0.111	0.206	1.862	0.928
40	0	53.1	0	41.0	23.4	100	0.105	0.111	0.209	1.876	0.938
45	0	52.8	0	41.1	23.7	100	0.105	0.111	0.209	1.896	0.944
50	0	53.2	0	42.2	23.6	100	0.104	0.111	0.206	1.891	0.936
55	0	52.9	0	43.0	23.5	100	0.105	0.111	0.210	1.883	0.943
60	0	53.3	0	44.2	23.8	100	0.104	0.111	0.204	1.902	0.933
120	0	56.2	0	50.3	24.4	100	0.098	0.111	0.173	1.955	0.876
180	0	56.7	6.7	53.4	24.6	93.3	0.093	0.104	0.167	1.964	0.892
240	0	56.3	7.8	55.9	24.7	92.2	0.093	0.103	0.169	1.972	0.905
300	0	56.4	8.8	56.9	24.4	91.2	0.092	0.102	0.171	1.951	0.909
360	0	56.9	9.4	58.6	24.3	90.6	0.091	0.101	0.168	1.935	0.899
420	0	56.7	11.1	59.6	24.8	88.9	0.090	0.099	0.165	1.982	0.912
480	0	56.7	12.5	61.1	24.7	87.5	0.090	0.098	0.166	1.968	0.918
540	0	55.6	13.7	61.5	24.4	86.3	0.091	0.096	0.178	1.948	0.949
720	0	56.1	14.6	61.9	24.8	85.4	0.090	0.095	0.170	1.979	0.942
1440	0	55.8	21.7	62.5	24.9	78.3	0.087	0.087	0.172	1.993	0.991
2880	0	56.6	28.4	60.5	24.7	71.6	0.081	0.080	0.166	1.970	1.013
5760	0	57.5	34.3	58.1	24.4	65.7	0.076	0.073	0.161	1.930	1.031
7200	0	57.9	36.6	54.9	24.9	63.4	0.073	0.071	0.153	1.981	1.038
10080	0	58.1	39.9	52.4	24.5	60.1	0.071	0.067	0.155	1.929	1.061
11520	0	58.6	40.6	51.9	24.9	59.4	0.070	0.066	0.147	1.987	1.051
12960	0	58.4	42.0	49.6	24.9	58.0	0.069	0.065	0.149	1.985	1.072
17280	0	59.2	44.8	48.5	24.7	55.2	0.066	0.062	0.144	1.955	1.074
18720	0	59.1	46.1	46.4	24.9	53.9	0.066	0.060	0.143	1.980	1.091
21600	0	59.4	46.1	46.0	24.8	53.9	0.065	0.060	0.141	1.971	1.080

Table S4. Time variation of **1**, $[PdPy*_4](BF_4)_2$, the $[Pd_3\mathbf{1}_6]^{6+}$ DWT, Py* and **Int**; $\langle a\rangle$–$\langle c\rangle$ values of the average composition of the intermediates ($[Pd_{\langle a\rangle}\mathbf{1}_{\langle b\rangle}Py*_{\langle c\rangle}]^{2\langle a\rangle+}$); the ($\langle n\rangle$, $\langle k\rangle$) values for the self-assembly of the $[Pd_3\mathbf{1}_6]^{6+}$ DWT from $[PdPy*_4](BF_4)_2$ ($[Pd]_0$ = 1.0 mM) and **1** ($[\mathbf{1}]_0$ = 1.0 mM) in CD_3NO_2 at 298 K with the initial stoichiometry of $[\mathbf{1}]_0/[Pd]_0$ = 1.0.

Time / min	**1** / %	$PdPy*_4$ / %	DWT / %	Py* / %	**Int** / %	$\langle a\rangle$	$\langle b\rangle$	$\langle c\rangle$	$\langle n\rangle$	$\langle k\rangle$
0	100	100	0	0	0	—	—	—	—	—
5	0	37.9	4.7	31.7	95.3	0.140	0.224	0.285	1.232	0.627
10	0	34.2	6.9	36.9	93.1	0.146	0.219	0.271	1.437	0.670
15	0	31.2	8.7	40.3	91.3	0.151	0.214	0.267	1.577	0.706
20	0	29.3	9.5	41.8	90.5	0.155	0.212	0.271	1.639	0.729
25	0	28.3	9.8	42.8	90.2	0.157	0.212	0.271	1.681	0.740
30	0	27.8	10.9	43.7	89.1	0.157	0.209	0.267	1.719	0.750
35	0	27.3	10.9	44.1	89.1	0.158	0.209	0.268	1.737	0.754
40	0	27.0	11.4	44.8	88.6	0.158	0.208	0.265	1.766	0.759
45	0	26.5	11.3	45.5	88.7	0.159	0.208	0.263	1.795	0.765
50	0	26.5	11.6	45.7	88.4	0.159	0.207	0.261	1.805	0.766
55	0	26.3	12.4	45.9	87.6	0.159	0.206	0.261	1.813	0.771
60	0	26.3	11.8	45.9	88.2	0.159	0.207	0.261	1.815	0.769
120	0	26.6	13.4	47.6	86.6	0.156	0.203	0.242	1.887	0.770
180	0	27.9	15.8	47.9	84.2	0.151	0.198	0.227	1.900	0.762
240	0	28.5	16.8	49.0	83.2	0.148	0.195	0.211	1.953	0.759
300	0	27.8	17.2	48.4	82.8	0.149	0.194	0.224	1.922	0.768
360	0	28.7	19.0	48.8	81.0	0.145	0.190	0.211	1.942	0.763
420	0	28.1	19.4	48.5	80.6	0.146	0.189	0.219	1.928	0.772
480	0	28.1	19.6	48.7	80.4	0.146	0.189	0.218	1.934	0.773
540	0	27.8	20.7	48.5	79.3	0.145	0.186	0.222	1.925	0.780
720	0	27.8	23.0	48.9	77.0	0.143	0.181	0.219	1.944	0.789
1440	0	28.6	26.9	49.5	73.1	0.136	0.172	0.206	1.970	0.793
4320	0	31.3	44.1	49.5	55.9	0.110	0.131	0.181	1.963	0.835
5760	0	31.9	48.3	49.5	51.7	0.103	0.121	0.174	1.965	0.849
7200	0	32.9	51.4	49.4	48.6	0.097	0.114	0.166	1.947	0.851
10080	0	33.8	56.6	49.6	43.4	0.089	0.102	0.156	1.964	0.873
11520	0	34.9	59.2	49.7	40.8	0.083	0.096	0.145	1.973	0.872
14400	0	35.8	62.9	49.8	37.1	0.077	0.087	0.136	1.974	0.883
15840	0	36.2	65.0	49.7	35.0	0.073	0.082	0.133	1.963	0.895
17280	0	36.1	64.4	49.6	35.6	0.074	0.084	0.134	1.957	0.891

Table S5. Time variation of **1**, $[PdPy^*_4](BF_4)_2$, the $[Pd_3\mathbf{1}_6]^{6+}$ DWT, Py* and **Int**; $\langle a\rangle$–$\langle c\rangle$ values of the average composition of the intermediates ($[Pd_{\langle a\rangle}\mathbf{1}_{\langle b\rangle}Py^*_{\langle c\rangle}]^{2\langle a\rangle+}$); the ($\langle n\rangle$, $\langle k\rangle$) values for the self-assembly of the $[Pd_3\mathbf{1}_6]^{6+}$ DWT from $[PdPy^*_4](BF_4)_2$ ($[Pd]_0$ = 1.0 mM) and **1** ($[\mathbf{1}]_0$ = 2.5 mM) in CD_3NO_2 at 298 K with the initial stoichiometry of $[\mathbf{1}]_0/[Pd]_0$ = 2.5.

Time / min	**1** / %	$PdPy^*_4$ / %	DWT / %	Py* / %	**Int** / %	$\langle a\rangle$	$\langle b\rangle$	$\langle c\rangle$	$\langle n\rangle$	$\langle k\rangle$
0	100	100	0	0	0	—	—	—	—	—
5	33.9	0	2.8	51.0	63.8	0.207	0.340	0.418	1.207	0.609
10	23.8	0	10.6	67.0	67.7	0.190	0.360	0.281	1.334	0.528
15	21.2	0	20.1	75.4	62.7	0.170	0.334	0.210	1.411	0.510
20	19.3	0	29.8	81.0	56.9	0.150	0.303	0.162	1.440	0.493
25	19.9	0	41.3	85.3	47.1	0.125	0.251	0.125	1.495	0.499
30	19.3	0	46.1	87.0	43.8	0.115	0.233	0.111	1.493	0.492
35	19.3	0	51.3	88.7	39.7	0.104	0.211	0.096	1.511	0.491
40	18.8	0	55.3	90.0	36.9	0.095	0.196	0.085	1.505	0.484
45	18.8	0	56.6	92.4	35.9	0.092	0.191	0.065	1.595	0.484
50	19.0	0	60.0	94.1	33.0	0.085	0.176	0.050	1.649	0.484
55	18.4	0	62.9	95.8	31.3	0.079	0.167	0.036	1.679	0.473
60	18.6	0	65.6	96.2	28.9	0.073	0.154	0.033	1.687	0.475
120	18.1	0	74.0	97.0	22.7	0.055	0.121	0.025	1.625	0.458
180	18.2	0	75.8	97.7	21.2	0.051	0.113	0.020	1.650	0.456
240	18.6	0	75.7	97.3	20.8	0.052	0.111	0.023	1.656	0.466
300	17.9	0	76.0	98.0	21.3	0.051	0.114	0.017	1.653	0.450
360	18.5	0	76.0	97.7	20.7	0.051	0.110	0.020	1.676	0.464
420	18.1	0	76.8	97.8	20.4	0.049	0.109	0.019	1.644	0.454
480	18.3	0	77.0	98.1	20.1	0.049	0.107	0.016	1.681	0.458
540	18.1	0	77.5	98.2	19.9	0.048	0.106	0.015	1.667	0.453

Table S6. Time variation of **1**, $[PdPy^*_4](BF_4)_2$, the $[Pd_3\mathbf{1}_6]^{6+}$ DWT, Py* and **Int**; $\langle a\rangle$–$\langle c\rangle$ values of the average composition of the intermediates ($[Pd_{\langle a\rangle}\mathbf{1}_{\langle b\rangle}Py^*_{\langle c\rangle}]^{2\langle a\rangle+}$); the ($\langle n\rangle$, $\langle k\rangle$) values for the self-assembly of the $[Pd_3\mathbf{1}_6]^{6+}$ DWT from $[PdPy^*_4](BF_4)_2$ ($[Pd]_0$ = 1.0 mM) and **1** ($[\mathbf{1}]_0$ = 4.0 mM) in CD_3NO_2 at 298 K with the initial stoichiometry of $[\mathbf{1}]_0/[Pd]_0$ = 4.0.

Time / min	**1** / %	$PdPy^*_4$ / %	DWT / %	Py* / %	**Int** / %	$\langle a\rangle$	$\langle b\rangle$	$\langle c\rangle$	$\langle n\rangle$	$\langle k\rangle$
0	100	100	0	0	0	—	—	—	—	—
5	40.2	0	7.0	73.5	56.3	0.221	0.536	0.253	1.181	0.413
10	38.6	0	21.1	89.1	50.9	0.188	0.484	0.103	1.338	0.388
15	40.3	0	35.7	94.1	41.8	0.153	0.398	0.056	1.395	0.384
20	43.5	0	53.4	95.2	29.8	0.111	0.284	0.046	1.405	0.391
25	44.6	0	58.7	97.3	26.0	0.098	0.248	0.026	1.482	0.397
30	45.8	0	63.8	98.8	22.2	0.086	0.212	0.011	1.574	0.407
35	46.1	0	65.3	99.2	21.2	0.083	0.202	0.007	1.600	0.409
40	46.4	0	67.2	99.2	20.0	0.078	0.190	0.007	1.602	0.410
45	46.1	0	69.1	99.6	19.4	0.074	0.185	0.004	1.574	0.398
50	46.2	0	70.9	99.8	18.4	0.069	0.175	0.002	1.575	0.397
55	46.4	0	71.4	99.6	17.9	0.068	0.170	0.004	1.576	0.399
60	47.2	0	73.2	99.7	16.2	0.064	0.154	0.003	1.636	0.414
120	47.9	0	78.8	99.5	12.7	0.050	0.121	0.005	1.636	0.419
180	47.1	0	80.3	99.7	12.8	0.047	0.122	0.002	1.524	0.386
240	47.7	0	82.1	99.9	11.3	0.043	0.107	0.000	1.587	0.398

References

(1) K. Suzuki, M. Kawano and M. Fujita, *Angew. Chem. Int. Ed.*, 2007, **46**, 2819–2822.

(2) T. Tateishi, W. Zhu, L. H. Foianesi-Takeshige, T. Kojima, K. Ogata and S. Hiraoka, *Eur. J. Inorg. Chem.*, 2018, 1192–1197.

(3) D. T. Gillespie, *J. Comput. Phys.* 1976, **22**, 403–434.

(4) D. T. Gillespie, *J. Phys. Chem.* 1977, **81**, 2340–2361.

(5) D. T. Gillespie, *Physica A*, 1992, **188**, 404–425.

(6) D. T. Gillespie, *Annu. Rev. Phys. Chem.* 2007, **58**, 35–55.